Integrative backstepping for one link manipulator quadrotor trajectory tracking

Reginaldo Cardoso[1], Rodrigo M. Morais[2], Éverton L. De Oliveira[1], Décio C. Donha[1]

[1]*Lab. of Dynamics and Control (LDC), Dept. of Mechanical Engineering, University of São Paulo (USP)*
Av. Prof. Mello Moraes, 2231, 05508-030, São Paulo-SP, Brazil
reginaldo.cardoso@usp.br, ev_lins@usp.br, decdonha@usp.br
[2]*Lab. of Dynamics and Control (LDC), Dept. of Mechatronic Engineering, University of São Paulo (USP)*
Av. Prof. Mello Moraes, 2231, 05508-030, São Paulo-SP, Brazil
rodmorais@usp.br

Abstract. The Unmanned Aerial Vehicle Manipulator (UAVM), is a robotic system formed by a UAV equipped with a manipulator and because of their high maneuverability and vertical takeoff and landing is possible to perform activities in small spaces. To face the dynamical coupling challenges, a mathematical model of the UAVM in the vertical plane is developed, considering a quadcopter UAV, with three degrees of freedom, equipped with a planar manipulator with one degree of freedom. The model is based on the classic Euler-Lagrange equation, considering the aerodynamic effects on the vehicle and the manipulator (drag forces), neglecting the effects of rotors on the manipulator. A backstepping control approach, divided into two sub controls, position control and attitude control, is studied. The controller is tested through numerical simulations for cases of passive and active manipulation, while the vehicle is tracking a trajectory. Movements of the vehicle with the manipulator locked showed the smallest errors in trajectory tracking. Both vehicle and manipulator moving simultaneously, make the error increase. Therefore, it is recommended that the vehicle only performs decoupled movements, avoiding sudden changes in the UAVM center of mass (CoM).

Keywords: UAVM, dynamic coupling, backstepping control

1 Introduction

Unmanned Aerial Vehicles Manipulator (UAVM), are robotic systems consisting of an unmanned aerial vehicle (UAV) equipped with at least one manipulator.

According to Meng et al. [1], aerial manipulators have gained a lot of attention since their initial appearance in 2010. That's because UAVMs are capable of performing several versatile manipulation functions in the air, considerably increasing their number of applications.

Despite its potential, the dynamic coupling between the UAV and the manipulator makes the system control really unstable. Zhang and He [2] consider the manipulator as a disturbance to vehicle control. In the dynamic model, disturbance is affected by variable inertia parameters of the aerial manipulator on which the robust control is build. Acosta et al. [3] study a non-linear control strategy to achieve greater precision and security in maintaining UAVM's stability while performing complex tasks. The solution combines a passive nonlinear dynamic controller for the UAV with a integral kinematic multi-task controller for the handler using an optimizer to define its relative motions. In Chen et al. [4] is proposed an adaptive tracking control strategy capable of dealing with two types of disturbances: Center of Mass (CoM) changes and external disturbances. By solving these problems, the UAVM would have a greater handling capacity for maintenance and transport tasks in the automotive industry. In Meng et al. [1] is shown a coordinated control for multiple UAVMs, based on a hierarchical three-layer architecture. The first layer is centered and defines the movement of the system, providing the desired movement of the center of mass of the system. The second and third layers are local to each UAVM, one receives the output references from the upper layer and calculates the movement of each vehicle, the other checks the success of the previous layer by making adjustments.

2 Mathematical Model

This simulation has with aims to observers the effect of the dynamic coupling of a UAVM, considered the mathematical model in the vertical plane. The model comprises a quadrotor vehicle. Assuming the two rotors that do not appear in the Figure 1 provide a constant force of a quarter of the weight of the UAVM. The manipulator is a cylindrical shape with length L and diameter D. In the end of the manipulator has a spherical mass of diameter d, which represents the end effector. The UAVM has four degrees of freedom, three related to the UAV (x, z and θ) and one to the manipulator (γ), which are represented with blue arrows in the Figure 1.

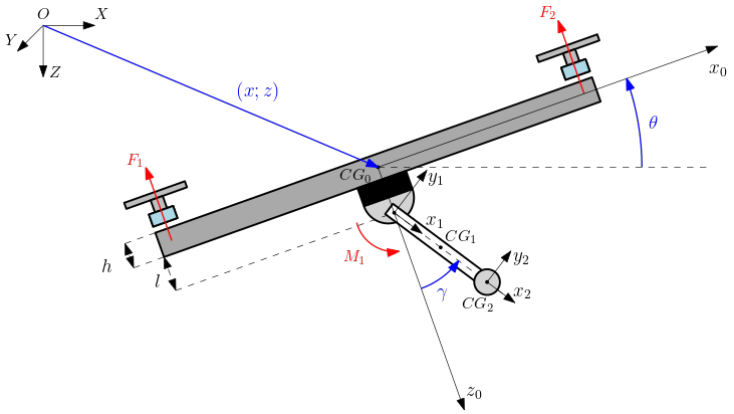

Figure 1. UAVM representation on the vertical plane.

Considering $\boldsymbol{q} = \begin{bmatrix} x & z & \theta & \gamma \end{bmatrix}^T = \begin{bmatrix} q_1 & q_2 & q_3 & q_4 \end{bmatrix}^T$ as the generalized coordinates of the system and $\boldsymbol{Q}$ as the non-conservative generalized force vector. The position of the vehicle coordinate center, $\boldsymbol{p}^N_{O_0} = \begin{bmatrix} q_1 & 0 & q_2 \end{bmatrix}^T$, then, it can be written the position vector of the vehicle's center of mass, $\boldsymbol{p}^N_{CG_0}$, the manipulator, $\boldsymbol{p}^N_{CG_1}$, and the mass, $\boldsymbol{p}^N_{CG_2}$,

$$\begin{aligned} \boldsymbol{p}^N_{CG_0} &= \boldsymbol{p}^N_{O_0} \\ \boldsymbol{p}^N_{CG_1} &= \boldsymbol{p}^N_{O_0} + \boldsymbol{R}^N_0 \cdot \begin{bmatrix} 0 & 0 & (h/2+l) \end{bmatrix}^T + \boldsymbol{R}^N_1 \cdot \begin{bmatrix} l_{CG_0|CG_1} & 0 & 0 \end{bmatrix}^T \\ \boldsymbol{p}^N_{CG_2} &= \boldsymbol{p}^N_{O_0} + \boldsymbol{R}^N_0 \cdot \begin{bmatrix} 0 & 0 & (h/2+l) \end{bmatrix}^T + \boldsymbol{R}^N_1 \cdot \begin{bmatrix} l_{CG_0|CG_2} & 0 & 0 \end{bmatrix}^T \end{aligned} \tag{1}$$

where $\boldsymbol{R}^N_0$ represents the rotation of the vehicle system to the inertial system, $\boldsymbol{R}^N_1$ the rotation from the manipulator system to the inertial system, $l_{CG_0|CG_1}$ and $l_{CG_0|CG_2}$ distance between the points CG_0 to CG_1, CG_0 to CG_2, respectively.

The velocity vector can be determined by the derivative with respect to time of eq. (1),

$$\begin{aligned} \boldsymbol{v}^N_{CG_0} &= \frac{d}{dt}(\boldsymbol{p}^N_{CG_0}) = \dot{\boldsymbol{p}}^N_{O_0} + \boldsymbol{\omega}^N_0 \times \boldsymbol{R}^N_0 + \boldsymbol{R}^N_0 \dot{\boldsymbol{p}}^0_{O_0|CG_0} \\ \boldsymbol{v}^N_{CG_1} &= \frac{d}{dt}(\boldsymbol{p}^N_{CG_1}) = \dot{\boldsymbol{p}}^N_{O_1} + \boldsymbol{\omega}^N_1 \times \boldsymbol{R}^N_1 + \boldsymbol{R}^N_1 \dot{\boldsymbol{p}}^1_{O_1|CG_1} \\ \boldsymbol{v}^N_{CG_2} &= \frac{d}{dt}(\boldsymbol{p}^N_{CG_2}) = \dot{\boldsymbol{p}}^N_{O_2} + \boldsymbol{\omega}^N_2 \times \boldsymbol{R}^N_1 + \boldsymbol{R}^N_1 \dot{\boldsymbol{p}}^2_{O_2|CG_2} \end{aligned} \tag{2}$$

where $\boldsymbol{\omega}^N_0$, $\boldsymbol{\omega}^N_1$, and $\boldsymbol{\omega}^N_2$ represent the angular velocity vectors in the inertial system,

$$\begin{aligned} \boldsymbol{\omega}^N_0 &= \begin{bmatrix} 0 & \dot{q}_3 & 0 \end{bmatrix}^T \\ \boldsymbol{\omega}^N_1 &= \begin{bmatrix} 0 & \dot{q}_3 + \boldsymbol{R}^N_1 \dot{q}_4 & 0 \end{bmatrix}^T \\ \boldsymbol{\omega}^N_2 &= \begin{bmatrix} 0 & \dot{q}_3 + \boldsymbol{R}^N_1 \dot{q}_4 & 0 \end{bmatrix}^T. \end{aligned} \tag{3}$$

The mathematical model was based on the classic Euler-Lagrange formalism, considering the aerodynamic effects of the vehicle and the manipulator (drag forces), but the drag force from the air displacement of the rotors in the manipulator was neglected.

The Lagrangian of the system $\mathcal{L} = \mathcal{T} - \mathcal{U}$, where $\mathcal{T}$ is the sum of the kinetic energy and $\mathcal{U}$ the sum of the energy potential, the Euler-Lagrange equation,

$$\frac{d}{dt}\left(\frac{\partial \mathcal{L}}{\partial \dot{\boldsymbol{q}}}\right) - \frac{\partial \mathcal{L}}{\partial \boldsymbol{q}} = \boldsymbol{Q}. \tag{4}$$

The system's kinetic energy is given by the sum of the rigid body kinetic energy of each part of the system. The kinetic energy of the vehicle is represented by ($i = 0$), the manipulator ($i = 1$) and the mass at the end of the manipulator ($i = 2$),

$$\mathcal{T} = \frac{1}{2}\sum_{i=0}^{i=2}\left(\dot{\boldsymbol{\eta}}_{CG_i}^{N}\right)^{T}\boldsymbol{M}_i\dot{\boldsymbol{\eta}}_{CG_i}^{N}, \tag{5}$$

where $\boldsymbol{M}_i$ = diag $([m_i \quad m_i \quad I_i])$ is the rigid body matrix, m_i being the mass and I_i being the moment of inertia of the i-th body, and $\dot{\boldsymbol{\eta}}_{CG_i}^{N}$=$\left[v_{CG_i,X}^{N} \quad v_{CG_i,Z}^{N} \quad \omega_{CG_i,Y}^{N}\right]^{T}$ is the absolute velocity vector.

The system's potential energy is given by the sum of the rigid body potential energy of each part of the system. The potential energy of the vehicle ($i = 0$), the manipulator arm ($i = 1$) and the mass at the end of the manipulator ($i = 2$),

$$\mathcal{U} = \sum_{i=0}^{i=2}\left(\boldsymbol{F}_{W_i}^{N}\right)^{T}\boldsymbol{p}_{CG_i}^{N}, \tag{6}$$

where $\boldsymbol{F}_{W_i}^{N} = \begin{bmatrix}0 & 0 & m_i g\end{bmatrix}^{T}$ the force weight vector, with g being the gravity acceleration vector.

Since the system is immersed in a fluid (air), there are drag forces influencing its movement. The function of drag forces can be determined by the following expression that uses the drag coefficient:

$$D = \frac{1}{2}\rho(\boldsymbol{C}_D\boldsymbol{A}_{ref})|V|V = \boldsymbol{K}|V|V, \tag{7}$$

where $\boldsymbol{C}_D$ is the drag coefficients of the vehicle and the manipulator, ρ represents the specific volume, V the velocity vector (vector formed by eq. (2) and eq. (3)) and $\boldsymbol{A}_{ref}$ the projected area of the system. Since $\boldsymbol{C}_D$, ρ, $\boldsymbol{A}_{ref}$ are constant parameters, it is possible to join them in a constant matrix $\boldsymbol{K}$ [5].

For subsequent implementation of the control, a variable ($\boldsymbol{U}_{control}$) is defined to represent the control input. Its expression is given by:

$$\boldsymbol{U}_{control} = \begin{bmatrix}U_x & U_z & U_\theta & U_\gamma\end{bmatrix}^{T} = \begin{bmatrix}-(F_z)\cos(q_3) & -(F_z)\sin(q_3) & M_\theta & M_\gamma\end{bmatrix}^{T} \tag{8}$$

where $F_z = F_1 + F_2$ represent the sum of motor forces, M_γ the moment generated at the joint between the vehicle and the manipulator and M_θ the moment generated by the motor forces. The generalized non-conservative force vector can be written as follows

$$\boldsymbol{Q} = \boldsymbol{D} + \boldsymbol{U}_{control}. \tag{9}$$

Substituting eq. (5), eq. (6) and eq. (9) into Equation 4, we obtain

$$\frac{d}{dt}\left(\frac{\partial \mathcal{L}}{\partial \dot{\boldsymbol{q}}}\right) - \frac{\partial \mathcal{L}}{\partial \boldsymbol{q}} = \boldsymbol{Q} \Longleftrightarrow \boldsymbol{M}(\boldsymbol{q})\ddot{\boldsymbol{q}} + \boldsymbol{f}(\boldsymbol{q}, \dot{\boldsymbol{q}}) = \boldsymbol{U}_{control}(\boldsymbol{q}), \tag{10}$$

isolating the term $\ddot{\boldsymbol{q}}$,

$$\ddot{\boldsymbol{q}} = \boldsymbol{M}(\boldsymbol{q})^{-1}\left[-\boldsymbol{f}(\boldsymbol{q}, \dot{\boldsymbol{q}}) + \boldsymbol{U}_{control}(\boldsymbol{q})\right], \tag{11}$$

where $\boldsymbol{M}(\boldsymbol{q})$ is the generalized mass and inertia matrix, $\boldsymbol{f}(\boldsymbol{q}, \dot{\boldsymbol{q}})$ is the matrix related to centrifugal, Coriolis and drag forces, $\boldsymbol{U}_{control}$ the control input vector associated with motor forces and joint torques.

Defining $\boldsymbol{x}_1 = \begin{bmatrix}x & z\end{bmatrix}^{T}$, $\boldsymbol{x}_2 = \begin{bmatrix}\dot{x} & \dot{z}\end{bmatrix}^{T}$, $\boldsymbol{x}_3 = \begin{bmatrix}\theta & \gamma\end{bmatrix}^{T}$, $\boldsymbol{x}_4 = \begin{bmatrix}\dot{\theta} & \dot{\gamma}\end{bmatrix}^{T}$, the model can be rewritten in the state space form $\dot{\boldsymbol{X}} = \boldsymbol{f}(\boldsymbol{X}, \boldsymbol{U})$,

$$\dot{\boldsymbol{X}} = \begin{bmatrix}\dot{x}_1\\ \dot{x}_2\\ \dot{x}_3\\ \dot{x}_4\end{bmatrix} = \begin{bmatrix}x_2\\ \boldsymbol{M}_2^{-1}\left[-\boldsymbol{f}_2 + \boldsymbol{U}_2\right]\\ x_4\\ \boldsymbol{M}_4^{-1}\left[-\boldsymbol{f}_4 + \boldsymbol{U}_4\right]\end{bmatrix} = \begin{bmatrix}x_2\\ \boldsymbol{\Delta f}_2 + \boldsymbol{U}_{2b}\\ x_4\\ \boldsymbol{\Delta f}_4 + \boldsymbol{U}_{4b}\end{bmatrix}. \tag{12}$$

3 Backstepping Control

To control the UAVM, a *backstepping* controller is chosen. Its development is based on the *Lyapunov* stability theory, to ensure the stability of the system. The control is divided in an attitude subsystem, responsible for controlling θ and γ, and a position subsystem, responsible for controlling x and y.

The Fig. 2 schematically shows the *backstepping* control used through a block diagram.

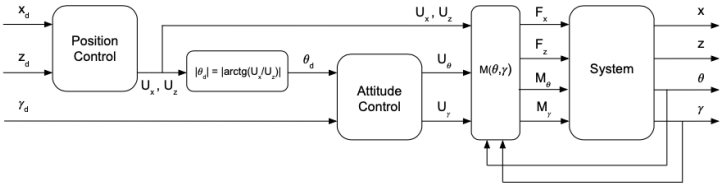

Figure 2. Representation of the controller's interaction with the vehicle.

The position control returns $\boldsymbol{U}_{2b} = \begin{bmatrix} U_x & U_z \end{bmatrix}^T$ and the attitude control returns $\boldsymbol{U}_{4b} = \begin{bmatrix} U_\theta & U_\gamma \end{bmatrix}^T$. To perform the decoupling of the state variables, the controller's outputs are multiplied by the matrix $\boldsymbol{M}(\theta, \gamma) = \begin{bmatrix} \boldsymbol{M_2}^{-1} & \boldsymbol{M_4}^{-1} \end{bmatrix}^T$ to get F_z, M_θ and M_γ. Finally, $\boldsymbol{U}_{control}$ is used to calculate the generalized coordinates through the model developed for the UAVM.

3.1 Position Control

First step is to define a proportional-integrative position error ($\boldsymbol{z}_1$),

$$\boldsymbol{z}_1 = \boldsymbol{e}_1 + \boldsymbol{\beta}_1 \int \boldsymbol{e}_1, \tag{13}$$

where $\boldsymbol{e}_1 = \boldsymbol{x}_1 - \boldsymbol{x}_{1d}$, with $\boldsymbol{x}_{1d}$ is the desired position vector, and $\boldsymbol{\beta}_1$ is a positive constant matrix.

Defining a new variable ($\boldsymbol{z}_2$) that is dependent on the virtual control variable ($\boldsymbol{\alpha}_1$)

$$\boldsymbol{z}_2 = \boldsymbol{x}_2 - \boldsymbol{\alpha}_1. \tag{14}$$

Considering the velocity error $\boldsymbol{e}_2 = \boldsymbol{x}_2 - \boldsymbol{x}_{2d}$, with $\boldsymbol{x}_{2d}$ is the desired velocity vector. Isolating the variable $\boldsymbol{x}_2$ from eq. (14), and substituting it in the velocity error, we obtain $\boldsymbol{z}_2 = \boldsymbol{e}_2 + \boldsymbol{x}_{2d} - \boldsymbol{\alpha}_1$. The derivative of eq. (13) can be written as follows,

$$\dot{\boldsymbol{z}}_1 = \boldsymbol{z}_2 - \boldsymbol{x}_{2d} + \boldsymbol{\alpha}_1 + \boldsymbol{\beta}_1 e_1. \tag{15}$$

The next step is defined a *Lyapunov* function. The function was chosen same as the [6]

$$\boldsymbol{V}_1 = \boldsymbol{z}_1^T \frac{1}{2} \boldsymbol{z}_1. \tag{16}$$

Following the backstepping procedure, it is necessary to ensure that the derivative of the function *Lyapunov* is negatively defined

$$\dot{\boldsymbol{V}}_1 = \boldsymbol{z}_1^T (\boldsymbol{z}_2 - \boldsymbol{x}_{2d} + \boldsymbol{\alpha}_1 + \boldsymbol{\beta}_1 \boldsymbol{e}_1), \tag{17}$$

the virtual control ($\boldsymbol{\alpha}_1$) is responsible for stabilizing $\boldsymbol{z}_1$ to zero,

$$\boldsymbol{\alpha}_1 = -\boldsymbol{K}_1 \boldsymbol{z}_1 + \boldsymbol{x}_{2d} - \boldsymbol{\beta}_1 \boldsymbol{e}_1, \tag{18}$$

where $\boldsymbol{K}_1$ is a positive diagonal matrix. The choice of $\boldsymbol{\alpha}$ was not able to guarantee the stabilization of $\boldsymbol{V}_1$

$$\dot{\boldsymbol{V}}_1 = -\boldsymbol{z}_1^T \boldsymbol{K}_1 \boldsymbol{z}_1 - \boldsymbol{z}_1^T \boldsymbol{z}_2, \tag{19}$$

the first term of eq. (19) is negative semi-defined because this term is equal to zero in the origin ($\boldsymbol{z}_1 = 0$), on the other hand, the second term can not be determined, so this second term must be eliminated to ensure that eq. (19) become negative-defined.

Considering the second *Lyapunov* function $\boldsymbol{V}_2 = \boldsymbol{V}_1 + \boldsymbol{z}_2^T \frac{1}{2} \boldsymbol{z}_2$, and its derivative can be calculated

$$\dot{\boldsymbol{V}}_2 = -\boldsymbol{z}_1^T \boldsymbol{K}_1 \boldsymbol{z}_1 - \boldsymbol{z}_1^T \boldsymbol{z}_2 + \boldsymbol{z}_2^T \left(\dot{\boldsymbol{x}}_2 - \dot{\boldsymbol{x}}_{2d} + \boldsymbol{K}_1 \left(\boldsymbol{z}_2 - \boldsymbol{K}_1 \boldsymbol{z}_1 \right) + \boldsymbol{\beta}_1 \left(\boldsymbol{z}_2 - \boldsymbol{K}_1 \boldsymbol{z}_1 - \boldsymbol{\beta}_1 \boldsymbol{e}_1 \right) \right) \tag{20}$$

Replacing $\dot{\boldsymbol{x}}_2 = \boldsymbol{\Delta f}_2 + \boldsymbol{U}_{2b}$ in Equation 20,

$$\dot{\boldsymbol{V}}_2 = -\boldsymbol{z}_1^T \boldsymbol{K}_1 \boldsymbol{z}_1 - \boldsymbol{z}_1^T \boldsymbol{z}_2 + \boldsymbol{z}_2^T \left(\boldsymbol{\Delta f}_2 + \boldsymbol{U}_{2b} - \dot{\boldsymbol{x}}_{2d} + \boldsymbol{K}_1 \left(\boldsymbol{z}_2 - \boldsymbol{K}_1 \boldsymbol{z}_1\right) + \boldsymbol{\beta}_1 \left(\boldsymbol{z}_2 - \boldsymbol{K}_1 \boldsymbol{z}_1 - \boldsymbol{\beta}_1 \boldsymbol{e}_1\right)\right), \quad (21)$$

for $\dot{\boldsymbol{V}}_2 < 0$, $\boldsymbol{U}_{2b}$ is chosen, with $\boldsymbol{K}_2$ being a constant positive diagonal matrix

$$\boldsymbol{U}_{2b} = -\boldsymbol{\Delta f}_2 + \dot{\boldsymbol{x}}_{2d} - \boldsymbol{K}_1 \left(\boldsymbol{z}_2 - \boldsymbol{K}_1 \boldsymbol{z}_1\right) + \boldsymbol{z}_1 - \boldsymbol{K}_2 \boldsymbol{z}_2 - \boldsymbol{\beta}_1 \left(\boldsymbol{z}_2 - \boldsymbol{K}_1 \boldsymbol{z}_1 - \boldsymbol{\beta}_1 \boldsymbol{e}_1\right). \quad (22)$$

Therefore, applying eq. (22) in eq. (21), we get that

$$\dot{\boldsymbol{V}}_2 = -\boldsymbol{z}_1^T \boldsymbol{K}_1 \boldsymbol{z}_1 - \boldsymbol{z}_2^T \boldsymbol{K}_2 \boldsymbol{z}_2 \quad (23)$$

the $\dot{\boldsymbol{V}}_2$ is a negative semi-defined function, which is enough to ensure the stability of the system.

3.2 Attitude Control

The same approach was used for the attitude control. The ending expression ($\boldsymbol{U}_{4b}$) of the control input can be written

$$\boldsymbol{U}_{4b} = -\boldsymbol{\Delta f}_4 + \dot{\boldsymbol{x}}_{4d} - \boldsymbol{K}_3 \left(\boldsymbol{z}_4 - \boldsymbol{K}_3 \boldsymbol{z}_3\right) + \boldsymbol{z}_3 - \boldsymbol{K}_4 \boldsymbol{z}_4 - \boldsymbol{\beta}_3 \left(\boldsymbol{z}_4 - \boldsymbol{K}_3 \boldsymbol{z}_3 - \boldsymbol{\beta}_3 \boldsymbol{e}_3\right) \quad (24)$$

where $\boldsymbol{K}_3$, $\boldsymbol{K}_4$, and $\boldsymbol{\beta}_3$ are positive constant matrix, and $\boldsymbol{e}_3 = \boldsymbol{x}_3 - \boldsymbol{x}_{3d}$ the attitude error with $\boldsymbol{x}_{3d}$ the desired attitude,

$$\boldsymbol{z}_3 = \boldsymbol{e}_3 + \boldsymbol{\beta}_3 \int \boldsymbol{e}_3 \qquad \boldsymbol{\alpha}_3 = -\boldsymbol{K}_3 \boldsymbol{z}_3 + \boldsymbol{x}_{4d} - \boldsymbol{\beta}_3 \boldsymbol{e}_3$$
$$\boldsymbol{e}_4 = \dot{\boldsymbol{e}}_3 = \boldsymbol{x}_4 - \boldsymbol{x}_{4d} \qquad \boldsymbol{z}_4 = \boldsymbol{x}_4 - \boldsymbol{\alpha}_3$$

4 Simulation

This section shows the numerical simulations carried out in MATLAB/Simulink® environment. Therefore, the behavior of the generalized coordinates (x, z, θ and γ) is compared with the references (x_d, z_d, θ_d and γ_d), both plotted in the same graphic. The desired trajectory was chosen that does not lead the actuators to saturation. Three scenarios are studied: the UAV movement, which only the vehicle is moving; the manipulator movement, which only the manipulator is moving; a composed movement, which the vehicle and the manipulator are moving. The vehicle and the controller parameters used are shown in Table 1.

Table 1. Simulation parameters

Parameter	Value	(Unit)	Parameter	Value	(Unit)
l_m	0.275	(m)	I_1	0.00136	$(kg \cdot m^2)$
h	0.015	(m)	I_2	0.0005	$(kg \cdot m^2)$
l	0.015	(m)	g	9.81	(m/s^2)
$l_{O_1\|O_2}$	0.240	(m)	C_{wx}	0.0148312416	(-)
$l_{O_1\|CG_1}$	0.120	(m)	C_{wz}	0.0123593680	(-)
m_0	1.477	(kg)	C_{mz}	0.0101286528	(-)
m_1	0.25	(kg)	C_{manx}	1.15	(-)
m_2	0.3	(kg)	C_{manz}	0.82	(-)
I_0	0.014641567	$(kg \cdot m^2)$	(-)	(-)	(-)
Controller parameters					
Position control			Attitude control		
$K_1 = K_2 = diag(0.167, 0.25)$			$2K_3 = K_4 = diag(5, 10)$		

Figure 3 shows the control result for $x_d = \sin(\omega t)$, $z_d = 0$ and $\gamma_d = 0$. Note that all states have a small oscillation at the start of the simulation. This oscillation occurs because of the vehicle under-actuated, which needs

to create a force component in the x's direction-axis. It occurs with an angle θ different from zero. Therefore, the γ angle needs to compensate for this variation in θ, it causing this oscillation in the initial moments. The controller shows can be able to follow the desired trajectory. Figure 4 shows the control result for $x_d = 0$, $z_d = 0$ and γ_d

Figure 3. First scenario, sinusoidal movement of the vehicle along the x-axis. Curve in magenta desired trajectory and curve in black UAVM simulation.

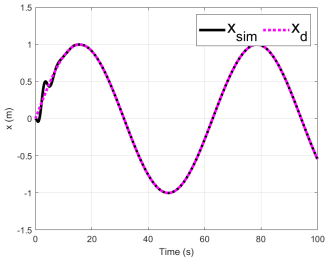

(a) UAVM response along the x-axis.

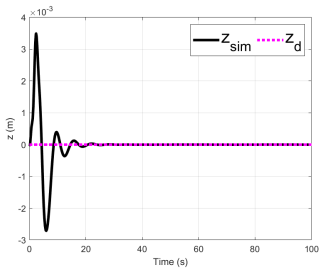

(b) UAVM response along the z-axis.

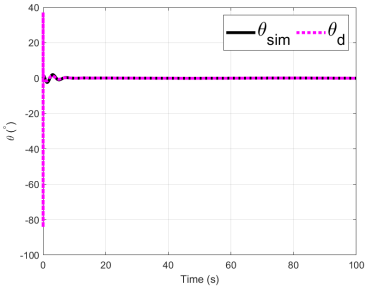

(c) UAVM response, θ angle.

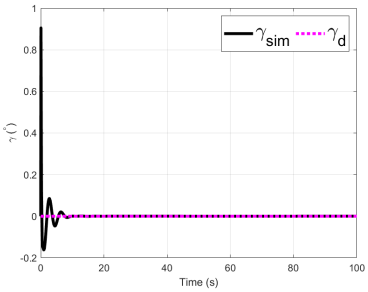

(d) UAVM response, γ angle.

starting with 0 going to $60°$ and coming back to 0. It can be seen that γ converges to the desired angle. But the theta angle needs to compensate for this movement. Because of the movement in gamma angle causes a change in the center's position of a mass of the UAVM. It causes oscillations in the other states, with a low amplitude (in the order of $\times 10^{-3} m$). Figure 5 shows the control result for $x_d = \sin(\omega t)$, $z_d = 0$ and γ_d starting with 0 going to

Figure 4. Second scenario, manipulator movement. Curve in magenta desired trajectory and curve in black UAVM simulation.

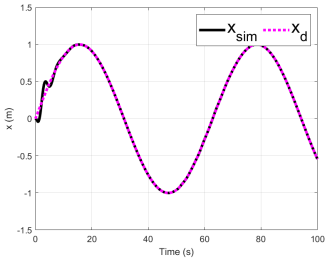

(a) UAVM response along the x-axis.

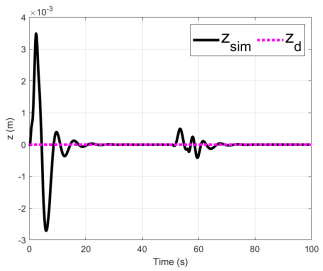

(b) UAVM response along the z-axis.

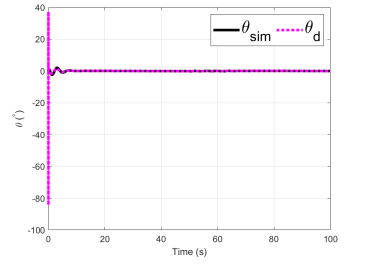

(c) UAVM response, θ angle.

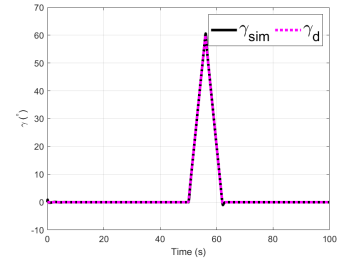

(d) UAVM response, γ angle.

$60°$ and coming back to 0. It can be observed that the compound movement, the z state, is the one that suffers the

most variations for the trajectory tracking.

Figure 5. Third scenario, composed movement. Curve in magenta desired trajectory and curve in black UAVM simulation.

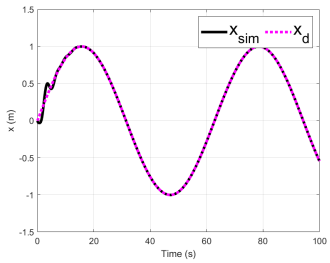

(a) UAVM response along the x-axis.

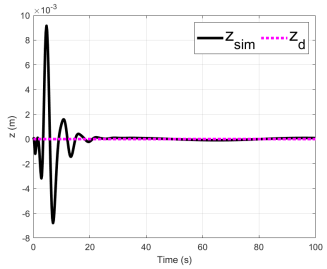

(b) UAVM response along the z-axis.

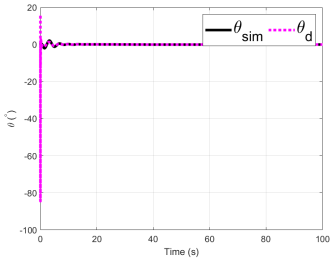

(c) UAVM response, θ angle.

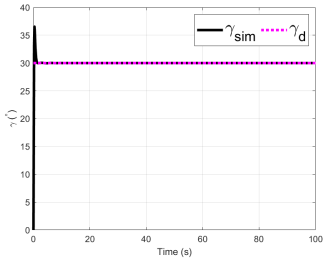

(d) UAVM response, γ angle.

5 Conclusion

The paper presents a dynamic model and backstepping control for a UAVM. The Euler-Lagrange based model considers drag forces as aerodynamic effects on the vehicle and the manipulator, its increasing dynamics complexities. The division of the controller into position and attitude showed be able to control the generalized coordinates. As validated above, the backstepping control has compensated for the effects of the dynamic coupling of the system and the drag force present in the manipulator model. Due to lack of space and by not adding any extra conclusions, the control efforts were not presented. In addition, during all the simulations, the control effort did not reach saturation.

Acknowledgements. The first and third authors acknowledge CAPES for the Ph.D. scholarships.

Authorship statement. The authors hereby confirm that they are the sole liable persons responsible for the authorship of this work, and that all material that has been herein included as part of the present paper is either the property (and authorship) of the authors, or has the permission of the owners to be included here.

References

[1] X. Meng, Y. He, and J. Han. Survey on aerial manipulator: System, modeling, and control. *Cambridge University Press*, vol. , 2019.
[2] G. Zhang and Y. He. Robust control of an aerial manipulator based on a variable inertia parameters model. *IEEE TRANSACTIONS ON INDUSTRIAL ELECTRONICS*, vol. , 2019.
[3] J. Acosta, de C. Cos, and A. Ollero. Accurate control of aerial manipulators outdoors. a reliable and self-coordinated nonlinear approach. *Elsevier Masson SAS*, vol. , 2020.
[4] Y. Chen, W. Zhan, and B. He. Robust control for unmanned aerial manipulator under disturbances. *IEEE Acsess*, vol. , 2020.
[5] T. F. Gomes. Numerical study of the flow between cylinders arranged side by side. (in portuguese). Dissertation (masters in materials integrity engineering), Faculty UnB Gama/FT/University of Brasília. In Portuguese, 2019.
[6] R. Cardoso, M. E. M. Meza, E. Rafikova, and S. L. M. C. Titotto. Backstepping and integrative sliding mode control for trajectory tracking of a hybrid remotely operated vehicle. In *2017 IEEE International Conference on Robotics and Biomimetics (ROBIO)*, pp. 116–121, 2017.